IEEE Access
Multidisciplinary | Rapid Review | Open Access Journal

Received April 22, 2021, accepted May 7, 2021, date of publication May 11, 2021, date of current version May 27, 2021.

Digital Object Identifier 10.1109/ACCESS.2021.3079292

Examination of Effective VAr With Respect to Dynamic Voltage Stability in Renewable Rich Power Grids

S. ALZAHRANI[1,2], (Member, IEEE), RAKIBUZZAMAN SHAH[3], (Member, IEEE), AND N. MITHULANANTHAN[1], (Senior Member, IEEE)

[1]School of Information Technology and Electrical Engineering, The University of Queensland, Brisbane, QLD 4072, Australia
[2]Electrical Engineering Department, Faculty of Engineering, Al Baha University, Al Bahah 65779, Saudi Arabia
[3]School of Engineering, Information Technology and Physical Sciences, Federation University Australia, Ballarat, VIC 3353, Australia

Corresponding author: S. Alzahrani (s.alzahrani@uq.edu.au)

ABSTRACT High penetrations of inverter-based renewable resources (IBRs) diminish the resilience that traditional power systems had due to constant research and developments for many years. In particular, dynamic voltage stability becomes one of the major concerns for transmission system operators due to the limited capabilities of IBRs (i.e., voltage and frequency regulation). A heavily loaded renewable-rich network is susceptible to fault-induced delayed voltage recovery (FIDVR) due to insufficient effective reactive power (E-VAr) in power grids. Hence, it is crucial to thoroughly scrutinize each VAr resources' participation in E-VAr under various operating conditions. Moreover, it is essential to investigate the influence of E-VAr on system post-fault performance. The E-VAr investigation would help in determining the optimal location and sizing of grid-connected IBRs and allow more renewable energy integration. Furthermore, it would enrich decision-making about adopting additional grid support devices. In this paper, a comprehensive assessment framework is utilized to assess the E-VAr of a power system with a large-scale photovoltaic power. Plant under different realistic operating conditions. Several indices quantifying the contribution of VAr resources and load bus voltage recovery assists to explore the transient response and voltage trajectories. The recovery indices help have a better understanding of the factors affecting E-VAr. The proposed framework has been tested in the New England (IEEE 39 bus system) through simulation by DIgSILENT Power Factory.

INDEX TERMS Dynamic voltage stability, effective VAr, high penetration, IBRs, load dynamics, LSPV, voltage recovery.

I. INTRODUCTION

Renewable energy has received widespread interest from individuals, organizations, and governments in the last two decades. The hope for clean, green, and affordable energy has significantly transformed the energy sector. The distribution network has been restructured, and there has been a major change in the concept of power flow. Roof-top PVs on residential and commercial buildings have become increasingly popular. Future grid features include active consumers, controllable loads, and bidirectional power flow. In the near future, transmission and sub-transmission networks may also experience a remarkable change. Many scattered inverter-based power plants would replace synchronous generator-based power plants. Several high-voltage direct currents (HVDC) and medium-voltage direct current (MVDC) lines would become the backbone of the network. Such a transformation in the power system may lead to operational issues related to power quality, stability, and security [1], [2].

With an emphasis on short-term profit-making, electrical power grids are often required to operate close to their limits. This may increase the risk of instability. Moreover, the significant replacement of synchronous generators (SGs) with inverter-based resources (IBRs), with limited reactive power ability, may cause voltage instability after fault-induced delayed voltage recovery (FIDVR). Without a comprehensive plan, the extensive integration of IBRs would reduce the stability and reliability of the system. Comprehensive planning would save resources that otherwise would be used to address

The associate editor coordinating the review of this manuscript and approving it for publication was Siqi Bu.

the consequences of increasing reliance on renewable energy. In the modern power system, stability is only determined by the physical characteristics of SGs. Such a system increasingly relies on the complex control of renewable generation, the range of system operating conditions, and the grid code by the transmission system operators (TSOs) [3].

Several studies have reported the dynamic voltage stability characteristics by considering load dynamics and dynamic VAr compensations [4], [6]. The primary reason for dynamic voltage instability in the system is the lack of reactive power support during the disturbances. The VAr support during the disturbance is known as the dynamic VAr or the effective VAr (E-VAr). E-VAr is usually less than the maximum VAr capability of the VAr resources due to limitations by complex network characteristics and operating conditions [7]. Maintaining short-term voltage stability (STVS) is one of the key issues for a renewable-rich stressed network due to the limited capability of IBRs to react to significant disturbance. Therefore, insufficient dynamic VAr being injected into the grid. Hence, the high penetrations of induction motors (IM) in a renewable-rich grid are more susceptible to STVS issues. In such a condition, a problem with STVS is a consequence of FIDVR caused by decelerating and stalling of IMs. Several research efforts have been made to investigate FIDVR, and various methods have been proposed for better E-VAr management. Paramasivam *et al.* [8] have developed an approach to optimally size and locate dynamic reactive resources to avoid short-term voltage instability. The research work in [9] was devoted to investigating the impact of large-scale photovoltaic (LSPV) power plant control strategies on grid voltage stability.

Moreover, an index called the voltage recovery index was proposed to measure the post-disturbance system response. Varma and Mohan [10] developed a novel day and night control scheme of LSPV which could mitigate FIDVR. The proposed method proved effective in improving STVS even though loads such as IMs are located far away from the PV power plant. The influence of PV dynamics on the grid STVS was also explored [11]. In this study, some countermeasures related to PV inverter operating conditions and dynamic voltage stability (DVS) capability were also examined and found suitable to enhance grid voltage stability.

Furthermore, an improved DVS capability was proposed in [11] through coordinating the injection of active and reactive power of the PV inverter as a function of the inverter terminal voltage. A clustered effective reactive reserve (CEQR) was proposed as a tool in determining the risk of dynamic voltage instability in [12]. The CEQR is useful in calculating the local E-VAr reserve and clustering system into separate areas for superior network control. An optimization method was supported for a dynamic reactive power reserve to enlarge the grid voltage security region [13]. This proposed method would help IBRs to be effective during any disturbances and avoids any cascading trip faults. Another operational planning tool for reactive power reserve management was presented in [14]. In this proposed method, the technical and economic aspects of the system were taken into account in determining the E-VAr reserve. A dynamic VAr planning technique was presented in [15] to enhance transient system stability and prevent failure recovery. Here, an index called transient voltage fluctuation (TVF) was proposed to evaluate the post-fault voltage profile. The TVF would thus be used to identify the best location for additional VAr devices.

The prior-mentioned works have explored system dynamic voltage stability, and several novel methods for reactive power reserve management have been proposed. Nevertheless, none of these studies have used each VAr resource contribution on system E-VAr during the sub-transient and transient time frame. Furthermore, t the sensitivity of E-VAr contribution to various system parameters such as dynamic load, PV penetration levels, integration location, load size, load VAr demand, and fault location were ignored in these works. The aim of this paper is to explore the system E-VAr from different dimensions and understand its influence on the transient response of the renewable-rich stressed grid.

In this research, the contributions of SGs, LSPV, and transmission lines on system E-VAr are systematically examined on a moderately complex multi-machine power system. The research focuses on extracting and demonstrate how VAr sources contribute to a renewable-rich power system under different load types and VAr demands. Several system aspects, which were overlooked in prior studies, have been considered to investigate their impacts on VAr resource. Moreover, the factors such as PV penetration level and integration location, load type, load size, VAr demand, bus SC level, and fault location were considered to work out the role of E-VAr on the post-disturbance voltage recovery performance of the system. This research thus contributes to a better understanding of each VAr source's contribution to the E-VAr. The main contributions of this paper can be summarized as follows:

- Propose a framework based on numerous indices with complementary characteristics to assess each VAr source contribution to system performance under supply and demand variations.
- Explore the influence of E-VAr on system transient response from the viewpoint of dynamic voltage stability under various operating conditions.
- Explore the influence of several factors on SGs contribution to the sub-transient and transient E-VAr.
- Explore the contribution of LSPV on system E-VAr under different integration locations.
- Determine the transmission line contribution to steady-state and dynamic performances of the system.
- Establish the relation between system characteristics and post-disturbance performance in the presence of IBRs considering short circuit level, E-VAr, and disturbance locations.

The simulation results clearly demonstrate the contribution of SGs, PVs, and transmission lines on system E-VAr. The results highlight their performance and contribution at different time frames under several operating conditions. Several

aspects can be improved during the planning and operational stages by considering the influence of VAr sources on system transient stability through the proposed framework.

The rest of this paper is organized as follows. The test system and modeling overview of various components, including the LSPV, are described in Section II. The research methodology, assessment indices, and assessment framework are presented in Section III. The steady-state and dynamic assessment results and discussions are given in Sections IV and V. The conclusions are dully drawn in Section VI.

II. MODELLING OVERVIEW

A. TEST POWER SYSTEM

The 10-machines 39 bus New-England power system, widely known as the IEEE 39 bus system, is used in this work as the test system [16]. A modification has been made to this system in order to observe the impact of LSPV power plants on the dynamic reactive power capability of a stressed or weak grid. Generally, the lesser amount of the fault current, the smaller theshort circuitratio (SCR). The weaker grids have a lower stability margin [17]. The IEEE 39 bus system can be divided into three zones, as illustrated in Fig. 1. Each zone has its own characteristics in terms of SC level (in MVA). For example, Zone 1 has the lowest average short-circuit (SC) level for load buses. On the other hand, Zone 3 has the highest SC level. Other zonal characteristics and their responses to system disturbances are explored in detail in the assessment section. The system has several SGs, as indicated in Fig. 1.

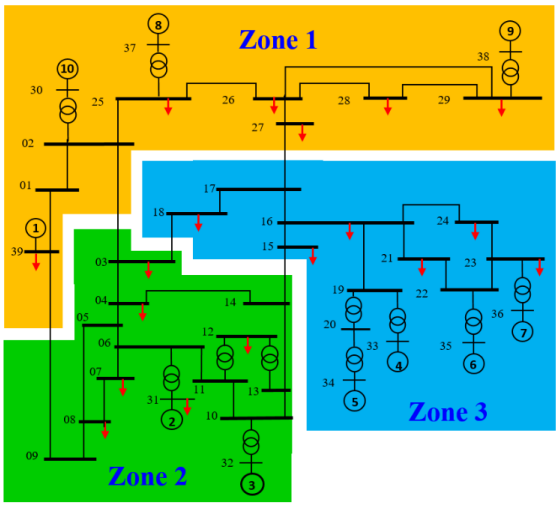

FIGURE 1. IEEE 39 bus test system [16].

B. GENERATOR MODEL

In IEEE 39 bus test system, there are ten machines. The SG 1 represents the connection to the rest of the system (the rest of the North American grid). Therefore, the detailed dynamic model of this machine was ignored. The rest of the SGs are modelled with their sub-transient and transient reactance. Generators 2 - 10 are equipped with IEEE Type 1 automatic voltage regulators. The speed governor is also considered for SG 2 - 10. Steam turbine governor (e.g., class IEEE Type G1) is used for SG 2 - 9. Generator SG 10 is equipped with a hydro turbine governor i.e., class IEEE Type G3. The MVA rating of SGs is not fully sufficient to equate SGs capabilities. Nevertheless, other parameters are introduced to identify the constraints on the dynamic performances of SG. For example, SG 9 is rated at 1000 MVA; however, transient reactance (*Xd'*) is almost double of SG 10. Therefore, it is expected that the SG 9 may have better dynamic performance and contribution compare to SG 9. Based on prior mention phenomena, some SGs could be classified as weak SG. Later, the influence of retiring such a generator and replacing them with IBRs is explored. The model of other power sources i.e. LSPV is mentioned in the following section.

C. LSPV MODEL

In this research, the Western Electricity Coordinating Council (WECC) LSPV plant model with the Electrical Control Model (REEC@backslasB) and the Generator-Converter Model (REGC@backslasA) is used [18]. Based on the grid code, the LSPV system should support system voltage by injecting or absorbing reactive power at the point of common coupling (PCC) [19]–[21]. This can be achieved by operating the PV inverters in voltage or reactive power control modes [22]. Other approaches can be used, such as installing static synchronous compensators (STATCOM), hybrid STATCOM, synchronous condenser or battery energy storage at the PCC with power factor, and active power-power factor operation of PV system [23]. However, more investigations are still required to identify the economic feasibility of such at the PV terminal.

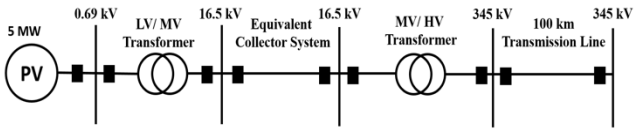

FIGURE 2. PV system layout.

Fig. 2 demonstrates the PV system layout. The PV inverter converts the DC power to a low voltage (LV) AC power at 0.69 kV. A 5 MVA medium voltage (MV) transformer is used to step up the voltage to 16.5 kV. Several PV units are connected through MV feeders to the main MV bus. The accumulative plant power is then directed through an MV/HV transformer to 345 kV. Hence, LSPV power plants are usually established far from the load center. Therefore, a 100 km transmission line is considered in this work between the PV plant and PCC.

In this work, the voltage control mode (VC) of the PV inverters is used to mimic the operational features similar to SG. The plant controller works to attain the PCC set voltage. This can be achieved by assigning the required VAr among

the PV inverters. The VAr contribution from PV depends on the current limit of the converter. The maximum converter current is normally selected as 1.5 times the rated current during the sub-transient and transient time frame. The current limit of the converter system comprises of active current (d-axis) and reactive current (q-axis) limit with relationship of $i_{lim} = \sqrt{i_{dlim}^2 + i_{qlim}^2}$

Different d and q axis current limits can be applied to the converter-based generator. A fixed d and q current limits have been used here. This means that the converter system remains connected to the system without injecting any additional reactive current. This is a widely used current limit logic in the literature. Three different current priorities can be used for such current limit logic. These can be stated as -

a) Active and reactive current have equal priority.
b) Active current has higher priority than reactive current.
c) Reactive current has higher priority than active current.

While designing the fixed current limiter in this paper, the active current is prioritized in the outputs of the current magnitude. The fixed current limit with active current priority can be defined by (1) & (2).

$$i_d^* = max\left(i_{lim}^*, i_{dref}^*\right) \tag{1}$$

$$i_q^* = max(\sqrt{i_{lim}^{*2} - i_q^{*2}}, i_{qref}^*) \tag{2}$$

Power system loads influence the ability of grid to respond to system disturbances. Therefore, load modelling is crucial.

D. LOAD MODEL

There are various loads in power systems, such as residential, commercial, and industrial loads. Those loads can be classified as either static or dynamic [24]. Each load exhibits distinct responses during the steady-state and transient time frame. It is impractical to represent the actual loads at each bus due to the uncertainty associated with load characteristics, time of operation, and complexity associated with such representation. Therefore, load modelling with an acceptable degree of accuracy is the common practice in power utilities. Several load models are being used for power system studies, such as exponential, polynomial or composite loads [24], [25] The composite load model is a commonly used model for dynamic stability studies [25]. The composite model combines the static and dynamic loads to precisely represent the relationship between the active and reactive power of the load and the bus voltage. Different approaches have been used for modelling load for dynamic studies. However, the use of a polynomial load model (ZIP load) in parallel to the induction motor (IM) (as depicted in Fig. 3) is the common practice in the North American utilities for dynamic studies [25].

Fig. 3 shows an equivalent circuit of a composite load model with equivalent IM and static loads. The IM was considered in this model as it is the dominant dynamic load in power systems, especially in industries. The total current (i) drawn at the substation is made up of the static (i_s) and dynamic (i_d) components as represented in (3) - (9). In the

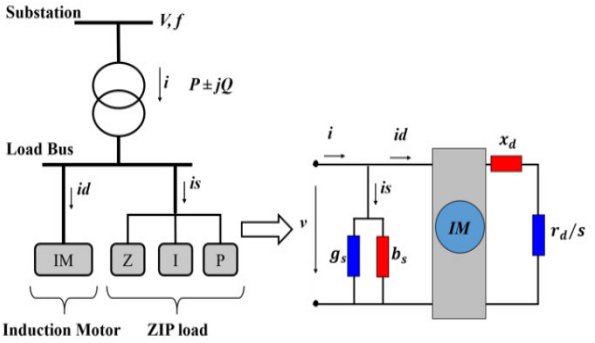

FIGURE 3. Composite load model.

static part, the conductance (g_s) and susceptance (b_s) can be expressed by (5) & (6), respectively. The dynamic part of the composite load is modelled as a simplified IM. Nevertheless, the modelling requirements depend on the investigation and the required accuracy level; other IM models with a higher degree of complexity can be used in composite load modelling with higher computational burden. However, the equivalent IM model given in Fig. 3 is reported suitable for dynamic studies in electro-mechanical time frame. In the IM model, the equivalent impedance (z_d) can be found from the respective rotor resistance (r_d) and reactance (x_d). The slip of the IM (s) can be found from the relationship between the electrical frequency (f_e) and the angular speed (ω_r) as in (8) & (9), where (T_m) is the mechanical torque and (T_e) is the electrical torque of IM. In FIDVR, IM stall as a result of low voltage condition. Stalled IM would affect the network adversely due to high demand of reactive power. Grid voltage would be significantly depressed for a few seconds after the fault is cleared before IM trips by the thermal protection (this could take from 3 to 20 seconds) [26].

$$i = i_s + i_d \tag{3}$$

$$i_s = v(g_s \frac{p}{p_0} + jb_s \frac{q}{q_0}) \frac{v_0^2}{v^2} \tag{4}$$

$$g_s = \frac{p_0}{v_0^2}(1 + t_{m0}) \tag{5}$$

$$b_s = -\frac{q_0 - p_0 t_{m0}(S_0/S_{cr})}{v_0^2} \tag{6}$$

$$i_d = \frac{v}{z_d} = \frac{v}{(r_d/S_0) + jx_d} \tag{7}$$

$$s = f_e - \frac{\omega_r}{2\pi} \tag{8}$$

$$\frac{d\omega_r}{dt} = \frac{T_e - T_m}{T_a} \tag{9}$$

The parameters of the composite load may influence the accuracy of stability studies. Nevertheless, according to the research effort reported in [27], the most influential parameters for the stability studies in the transient timeframe are the size of the load (P_0), the normal operating slip (S_0), critical slip (S_{cr}), the proportion of the dynamic load (t_{m0}), and the acceleration time constant (T_a). In this work,

recommended values suggested by various TSOs are considered for the composite load modeling. Parameters presented in Table 1 resulted from a case study reported in [28] have been used in this paper.

TABLE 1. Parameters of composite load model [28].

PARAMETERS	p_1	p_2	p_3	q_1	q_2	q_3	s_0	s_{cr}	T_a(S)
VALUE	0.552	0.338	0.110	0.599	-1.427	1.828	1.35	10.29	0.93

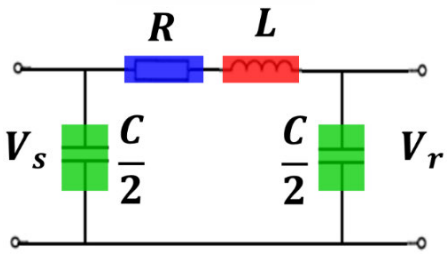

FIGURE 4. Line nominal Pi (Π) model.

E. TRANSMISSION LINE MODEL

The New England system contains 34 high voltage (HV) transmission lines ranging from 10 km to 248 km in length. According to the standard transmission line classification, there are 20 short lines, 13 medium lines, and one long line. Different line models can be used to represent these lines. Nevertheless, as this investigation aims to account for the overall VAr contribution from the lines, a standard π equivalent circuit is used (as shown in Fig. 4). In each line, with regard to reactive power flow, there would be reactive power (Q_{line}) consumed by the line reactance (X_L) and reactive power (Q_c) generated by the line shunt capacitance (C). The Q_{line} is directly proportional to the square of the line current as in (10). On the other hand, Q_c is directly proportional to the square of the line voltage (V) and system frequency (f) as in (11). Charging current (I_c) is injected into the system caused by line shunt capacitance as given in (12). The line shunt capacitance has resulted from the potential difference between transmission line conductors, which allows them to charge like capacitors. The size and separation distance of conductors influence the line effective capacitance.

In the 39 bus system, the line capacitances vary between 0.006-0.027 μF/km. The total capacitance of the line is in the range of 0.1-2.67 μF. The system loading conditions affect the Q_{line} and Q_c. The overall reactive power status of the line i.e., line net VAr (Q_{net}) can be obtained as in (13). During the light loading condition, the line would have a surplus of Q_{net} as Q_c would be greater than Q_{line}. However, a heavily loaded transmission line would have a deficit of Q_{net}. The status of the Q_{net} would affect the system steady-state and dynamic performance as the existence of sufficient VAr influences the static and dynamic voltage stability.

$$Q_{line} = I^2 X_L \tag{10}$$

$$|Q_c| = 2\pi f C V^2 \tag{11}$$

$$I_c = 2\pi f C (V/\sqrt{3}) \tag{12}$$

$$Q_{net} = Q_c - Q_{line} \tag{13}$$

III. METHODOLOGY

A. ASSESSMENT INDICES

For a renewable rich network with high penetration of IM loads, a voltage recovery performance of the load bus is a crucial aspect towards voltage stability [9]. Several indices have been used to evaluate the voltage recovery, such as voltage deviation index (VDI), improved voltage stability index (IVSI), and voltage stability factor (VSF), and others [29]. In this research, the voltage recovery index (VRI) has been considered [9]. Hence, the VRI reflects all transient periods considered in this paper. Other indices i.e., steady-state VAr (SS-VAr), sub-transient VAr (ST-VAr), and transient VAr (T-VAr), and voltage recovery time (VRT) are also used. These indices would help in evaluating the contribution of each VAr source on voltage recovery at a specific post fault time frame. The combination of these indices is useful in sizing the LSPV plant, justify the requirement of additional VAr, their optimal size, and their location for other VAr resources as well as the optimal tuning of the coordinated control method of the LSPV and other VAR resources.

1) VOLTAGE RECOVERY INDEX (VRI)

The FIDVR phenomenon had been investigated in [9]. An index called VRI was proposed to explore the STVS of the system analytically. Moreover, VRI examines the system's transient response under different control methods in the presence of IBRs. The WECC voltage recovery criterion is used as a point of reference for the post-fault performance calculation, as depicted in Fig. 5.

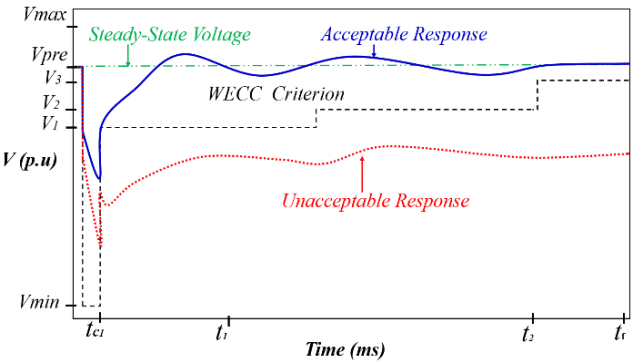

FIGURE 5. Voltage recovery index VRI [9].

The numerical outcome of VRI is in the range of $[-1, 1]$. If a load bus returns to its pre-fault value once the fault is cleared, a VRI would be 1. In contrast, if the bus voltage collapse after removing the disturbance, a VRI would be -1. The VRI would be equal to zero if voltage recovery only meets the WECC minimum voltage recovery criterion. The following pseudocode briefly outlined the main steps to

evaluate the voltage recovery of the load bus. The parameters used in finding the VRI are defined in Table 2.

Step-1: Define the voltage violation criteria as in (14).
Step-2: Divide the voltage between V_{max} and V_{min} into L samples.
Step-3: Define the probability density function p^{VRI+}& p^{VRI-} of the voltage samples.
Step-4: Apply the weighting function (η_j^+)& (η_j^-) for the post-fault voltage as in (15) & (16).
Step-5: Calculate the VRI according to (17).

TABLE 2. Parameters used in the definition of VRI.

PARAMETER	DEFINITION	UNIT
V_{WECC}	VOLTAGE VIOLATION CRITERIA OF WECC	[P.U.]
V(T)	VOLTAGE CURVE DURING THE TRANSIENT TIME	[P.U.]
V_{PRE}	PRE-FAULT STEADY-STATE VOLTAGE	[P.U.]
V_{MIN}	DISTURBANCE MINIMUM VOLTAGE	[P.U.]
V_{MAX}	POST DISTURBANCE MAXIMUM VOLTAGE	[P.U.]
V_1	VOLTAGE LIMIT 1 OF WECC VIOLATION CRITERION	[P.U.]
V_2	VOLTAGE LIMIT 2 OF WECC VIOLATION CRITERION	[P.U.]
V_3	VOLTAGE LIMIT 3 OF WECC VIOLATION CRITERION	[S]
T_{C1}	TIME AT FAULT CLEARING INSTANT	[S]
T_1	TIME LIMIT 1 OF WECC VIOLATION CRITERION	[S]
T_2	TIME LIMIT 2 OF WECC VIOLATION CRITERION	[S]
T_F	END OF TRANSIENT OBSERVATION TIME	[S]
L	TOTAL NUMBER OF VOLTAGE SUB-INTERVALS	[-]
A	TOTAL NUMBER OF VOLTAGE SAMPLES	[-]
M	TOTAL NUMBER OF VOLTAGE CONSTRAINTS	[-]

The VRI is a local index which expresses each load bus voltage transient performance. A global voltage recovery index VRI_{sys} has been proposed recently in [30] to measure the network strength and overall performance from the viewpoint of short-term voltage stability. The grid code defines the voltage limits for the low voltage ride through LVRT capability. In this research, the WECC voltage criteria were considered in calculating the VRI. The V_{WECC} states that following an N-1 contingency, the system voltage should not exceed its pre-fault value by 25% and 30% for all load and non-load buses, respectively. Moreover, a voltage dip time limit has been mentioned in V_{WECC} where the load bus voltage should not dip more than 20% of its normal value for more than 20 cycles [31]. The minimum acceptable voltage and duration are defined according to the V_{WECC} envelope as in (14). The value of voltage limits and the corresponding time limits are presented in Table 3. The weighting function is used to reward (η_j^+) or to penalize (η_j^-) the transient voltage based on the pre-fault voltage profile. The value of the weighting function, i.e., η_j^+&η_j^- are calculated based on (15) & (16). Where λ_j^+&λ_j^- define the width of the weighting function, and j&i are defined by the total number of voltage constraints (M) and the total number of sub-intervals (L).

$$V_{WECC} = \begin{cases} V(t) \geq V_1 \text{ for } t_{c1} \leq t \leq t_1 \\ V(t) \geq V_2 \text{ for } t_1 \leq t \leq t_2 \text{ and } V_2 > V_1 \\ V(t) \geq V_3 \text{ for } t_2 \leq t \leq t_f \text{ and } V_3 > V_2 \end{cases} \quad (14)$$

$$\eta_j^+ = e^{-\lambda_j^+ (V_i - V_{pro})^2} \quad (15)$$

$$\eta_j^- = e^{-\lambda_j^- (V_i)^2} \quad (16)$$

$$VRI = \frac{1}{A} \sum_{j=1}^{M} \sum_{i=1}^{L} \left(\eta_{ji}^+ p_{ji}^{VRI+} + \eta_{ji}^- p_{ji}^{VRI-} \right) \quad (17)$$

TABLE 3. VRI parameters values [9].

PARAMETER	V_1 [P.U]	V_2 [P.U]	V_3 [P.U]	T_{C1} [S]	T_1 [S]	T_2 [S]	T_F [S]
VALUE	0.75	0.8	0.95	1.1	1.8	3.5	4

2) VOLTAGE RECOVERY TIME (VRT)

The voltage recovery index summarizes the transient response of the load bus over a few seconds. Such an index is not sufficient to explore the E-VAr contribution of IBRs and their impact on the dynamic response of the system. It is essential to examine the bus performance during the first few cycles after the fault is cleared. After the post fault, the time required to reach the voltage to a certain level of pre-fault value is referred to as VRT. The VRT highlights the system response in the transition stage from sub-transient to transient, where FIDVR commonly occurred. Therefore, paying more attention to the first few cycles after the fault clearance would identify the area of influence of PV integration. Moreover, the VRT may be used to propose a mitigation solution such as dynamic VAr support to improve system voltage recovery when IBRs are being integrated into the network.

3) EFFECTIVE REACTIVE POWER OF VAR SOURCES (E-VAR)

In a power system, reactive power is essential for the network to keep the steady-state and the transient voltage within an acceptable limit. Reactive power is primarily supplied by the SGs. Nevertheless, if SGs' capabilities are insufficient to meet the grid VAr requirements, other VAr resources could be installed in specific locations.Transmission line capacitances also contribute slightly to the system VAr. However, line VAr is not controllable such as SGs VAr. The maximum steady-state and dynamic VAr capability of SG could be determined by its MVA rating, synchronous, sub-transient, and transient reactance. SGs would not always generate their maximum VAr in practical situations due to the VAr flow constraints in the network.In other words, E-VAr from SGs could be less than the full VAr capability of SGs. This research aims to investigate the E-VAr capability of VAr resources in steady-state and transient time frames under various operating conditions.

The E-VAr of each VAr source can be assessed by estimating their VAr output. Figure 6 shows a typical VAr of SG before, during, and after the fault. The VAr contribution could be categorized into three types: steady-state VAr (SS-VAr), sub-transient VAr (ST-VAr), and transient VAr (T-VAr). These VArs differ from each other in terms of the magnitude and time frame. During the steady-state, the SGs or other VAr sources inject the required VAr to regulate the

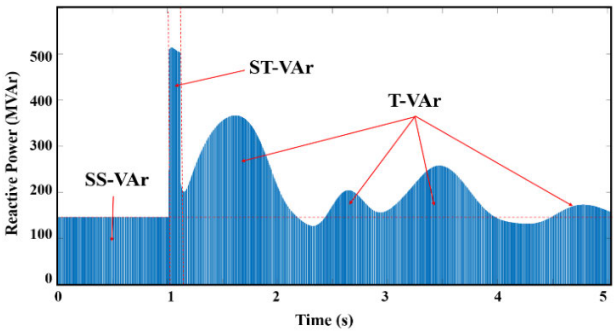

FIGURE 6. SG typical VAr.

grid voltage. The synchronous reactance of the generator influences the SS-VAr of SGs. Accordingly, each SG has a maximum VAr capability predefined in its P-Q capability curve. Once a disturbance occurs, for instance, a three-phase fault, a ST-VAr would be injected to prevent system instability. In this type of VAr, the SGs have an immediate response to the SC, and a fault current increases to 4-6 times of the SG rated current. The sub-transient VAr can last for a few cycles (milliseconds). The sub-transient reactance of each SG and the electrical distance from the fault location influence the amount of fault current injection during the fault. In contrast, the transient VAr lasts for few seconds after the disturbance is cleared. The transient reactance of SG governs the SG response in this type of VAr. Finally, and for a stable system, after a few seconds of disturbance, the SG should return to its pre-fault SS-VAr or a new steady-state if the disturbance causes some outage in the system [32].

The E-VAr determining processes are carried out by estimating the area under the curve of the output VAr as in Fig. 6. By using (16), the amount of E-VAr injected in each time frame would be found where a and b define the VAr type boundaries and t is the time in ms. The SS-VAr is flat and uniformly distributed across the steady-state time frame. The ST-VAr is almost uniformly distributed during the fault period, assuming the fault is cleared within a few cycles. The T-VAr is fluctuating and non-uniformly distributed during the transient period. Due to transient VAr's non-uniformity, an average VAr of that period is used to evaluate the E-VAr under different load types and loading conditions for simulation scenarios.

$$E - VAr = \int_a^b VAr\,(t)\,d(t) \tag{18}$$

The E-VAr index is more applicable in system planning stages and achievable in a simulation-based environment. The E-VAr index would help explore the grid impact of renewable integration via highlighting the system post-fault performance in the presence of renewable resources. Moreover, E-VAr could be used to justify the need for additional VAr resources and a guideline in sizing and placing the additional VAr. Furthermore, with the application of AI-based network parameter estimation, E-VAr could be used by the grid operators as an online tool in managing and controlling system VAr source in operation planning stage.

B. SIMULATION SCENARIOS

To achieve the research aim, several simulation scenarios depicted in Table 4 have been used for the simulation studies. The simulation scenarios would help understand the contribution of SGs, PV, and transmission lines in E-VAr under different operation conditions. These scenarios are grouped into three.

TABLE 4. Simulation scenarios.

Group	Scenario #	SGs %	PVs %	VAr demand %	Load type	
					Static	Dynamic
A	1	100	0	100	X	
	2	100	0	120	X	
	3	100	0	100		X
	4	100	0	120		X
B	5	80	20	100	X	
	6	80	20	120	X	
	7	80	20	100		X
	8	80	20	120		X
C	9	80	20*	100	X	
	10	80	20*	120	X	
	11	80	20*	100		X
	12	80	20*	120		X

* Three LSPV (360 MW each) connected to bus 4, 16 & 27.

The first scenario (i.e., Group A) is the base case without LSPV. This group is used to explore the influence of integration LSPV in system E-VAr. The second group of scenarios (i.e., Group B) includes 20%LSPV power plants.The LSPVs are integrated at the same HV buses of SGs 3-9, and the MVA ratings of SGs are reduced by 20The last case (i.e., Group C) would have 20% PV power plants integrated equally into the three areas: buses 4, 16, and 2. Similar to Group B, the MVA ratings of SGs are reduced by 20%. Group C differs from group B by integrating the PVs into the load center through a 50 km transmission line. Integration PVs to the load centers would cause a change in system power flow that would impact line reactance-related VAr. Therefore, the line net VAr would be altered. Analysing the scenarios in the second and third groups would help in exploring the impact of PV integration location in system E-VAr. In all of these scenarios, system E-VAr would be explored under two different load types, i.e., static and dynamic. Finally, the impact of distributed generation, such as rooftop PV, would be examined by increasing load VAr demand by 20%. This would allow investigating the influence of increasing load VAr demand in SG, PV, and line steady-state, sub-trainset, and transient E-VAr.

C. ASSESSMENT FRAMEWORK

Figure 7 illustrates the flowchart of the proposed assessment framework. The steady-state assessment includes power flow and SC calculations. The dynamic evaluation is then carried out to explore the system responses during the fault and

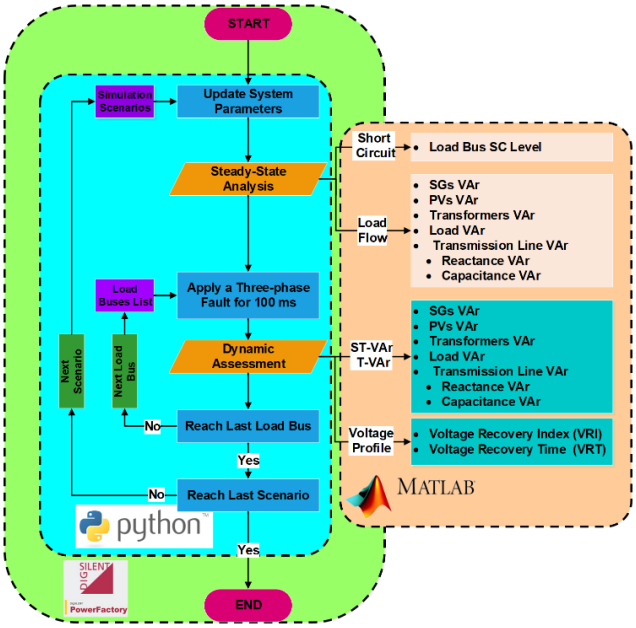

FIGURE 7. Flowchart of the proposed framework.

post-fault for different operating conditions. Python programming has been utilized to automate the time-domain simulation in which the PV penetration levels and load types, and load VAr demands are adjusted in each simulation loop. MATLAB is used tocalculate the system E-VAr and post-fault performance indices. The outcome of the steady-state and dynamic assessments are used to explore the system contribution in E-VAr for different time frames and under different operating scenarios. Moreover, the assessment of system recovery and dynamic VAr support under different operation conditions would help understand the degree of correlation between the system performance and the system component contributions towards system E-VAr.

IV. STEADY-STATE ASSESSMENT

The steady-state assessment of VAr flow would explore each VAr source contribution to the system SS-VAr for differentoperating conditions. Moreover, this assessment also examines the influence of LSPV integration on SS-VAr of transmission lines. The SS-VAr is independent of load types that means static load and dynamic load would consume the same amount of SS-VAr. On the other hand, the load type effect of load types on bus recovery can be seen during the transient period.

A. STEADY-STATE VAr

Figure 8 demonstrates the SS-VAr associated with VAr sources and sinks. The SGs and capacitances of the transmission lines are the only sources of VAr in Group A scenarios. SGs contribute 51% of the total injected VAr while the line share is 49%. The loads consume more than two-thirds of injected VAr.Transformers reactances and transmission line reactances consume 12% and 17% of systems SS-Var,

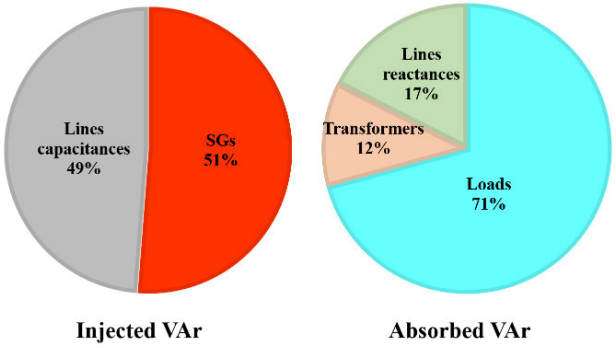

FIGURE 8. Total injected and absorbed steady-state VAr.

respectively. In Group A scenarios, the transmission lines have a surplus net VAr of 760 MVAr. The impact of the growth in VAr demand on the participation of VAr sources and sink is explored in the next section.

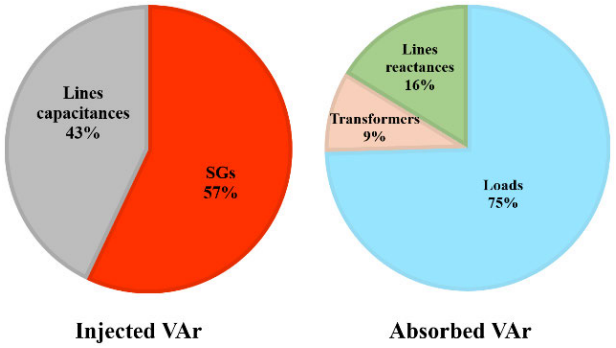

FIGURE 9. Steady-state VAr with 20% growth on load VAr.

B. IMPACT OF LOAD VAr GROWTH

Load VAr growth would affect the system power flow. The SS-VAr map would be altered, as shown in Fig. 9. The lines VArs are not controllable. Therefore, it is not possible to inject more VAr from the lines. However, SGs have the capability to meet the growth by injecting more VAr. In this case, SGs share of VAr increased to 57% while line share drops to 43%. However, more VAr injection from SGs may increase the line reactive power consumption. As a result, the transmission line net VAr would be reduced by 4%.

C. IMPACT OF PV INTEGRATION

In this section, the impact of LSPV integration on reactive power has been explored in Groups B and C. As presented in Fig. 10, PV integration would contribute slightly to the generated VAr. Moreover, when there is more VAr demand, the PV would contribute more, as in Scenarios 6 and 9. It should be noticed that the voltage set-point governs VAr since PV is operating in the voltage control mode. In this research, a voltage set-point was 1.02 p.u. However, different voltage set-points would result in different injections and absorption of VAr according to VAr demand at PCC. With the Group C scenarios, integration of LSPVs to the load centers through

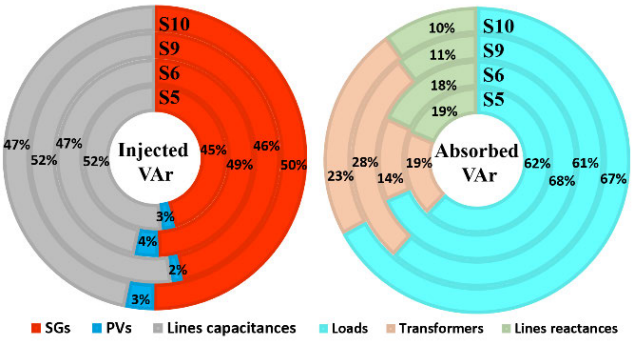

FIGURE 10. Steady-state VAr with 20% PV.

50 km transmission lines would substantially affect the power flow. Nearly 20% of the power would be injected from LSPV. Therefore, the transmission line reactance losses were reduced significantly. On the other hand, the total consumed VAr of transformers would be almost doubled. The lines net VAr surpluses would be increased by approximately 25%.

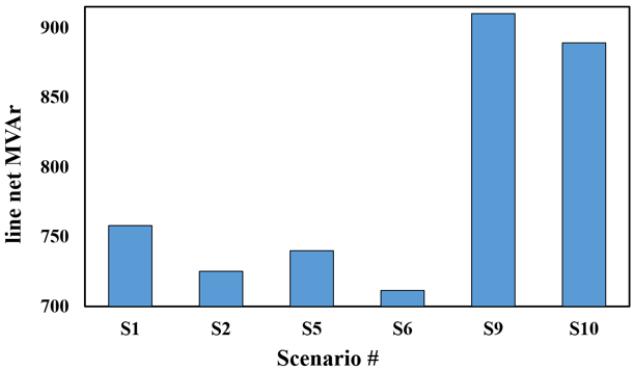

FIGURE 11. Transmission lines net VAr.

Fig. 11 shows the net VAr in transmission lines under various scenarios. Only scenarios (S1, S2, S5, S6, S9, and S10) with static load types are presented since the relevance of dynamic load in static analysis is minimal. It is evident that PV integration location affects the net VAr of the lines. The largest net VAr (180 MVAr greater than the base case) has occurred under scenario 9. The lowest net VAr (96% from the base case) is observed under Scenario 6, i.e., with 20% PV and 120% VAr demand growth.

V. DYNAMIC ASSESSMENT

The dynamic assessment examines the system response after it is subjected to the disturbance. Network voltage recovery has a high priority in the post-fault performance. Otherwise, delayed voltage recovery may result in voltage or angular instability. In this research, the impact of different operating conditions on the transient response of the system is examined. The examination involves looking at each VAr source contribution during and after the disturbance in terms of their injected E-VAr. Two types of load and their transient responses with VAr growth would be considered. Moreover, the influence on E-VAr of integrating LSPV at various locations is taken into account.

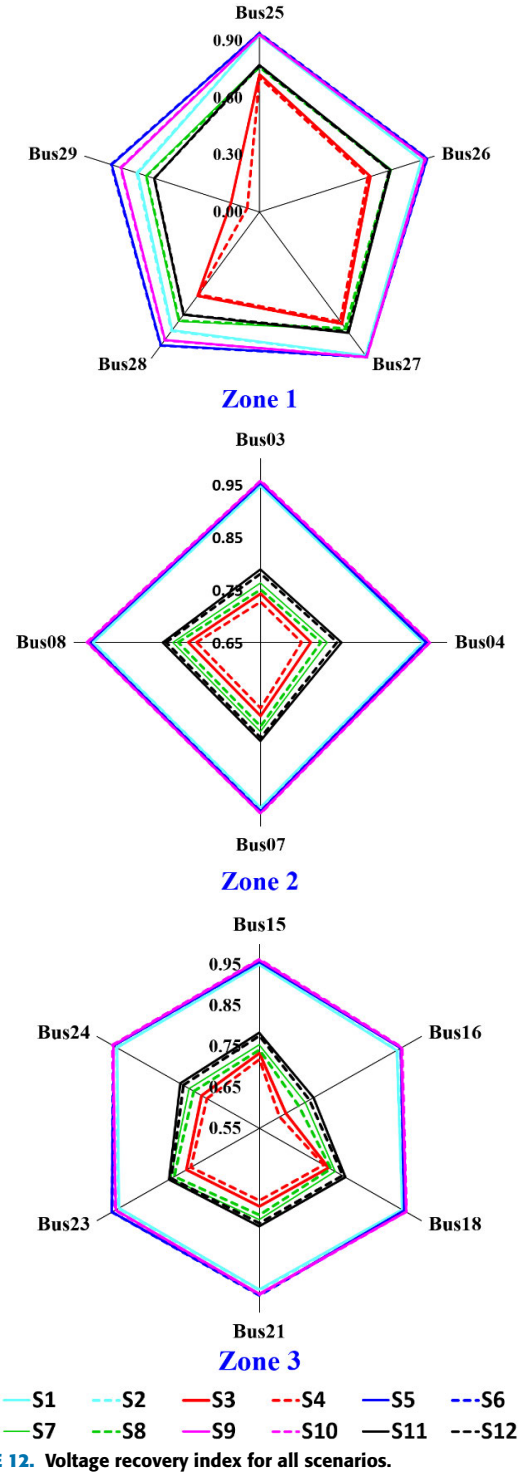

FIGURE 12. Voltage recovery index for all scenarios.

A. LOAD BUS PERFORMANCE

The VRI is used to evaluate the transient response of load buses after a 100 ms three-phase fault. Fig. 12 shows the VRI of load buses for the simulation scenarios.

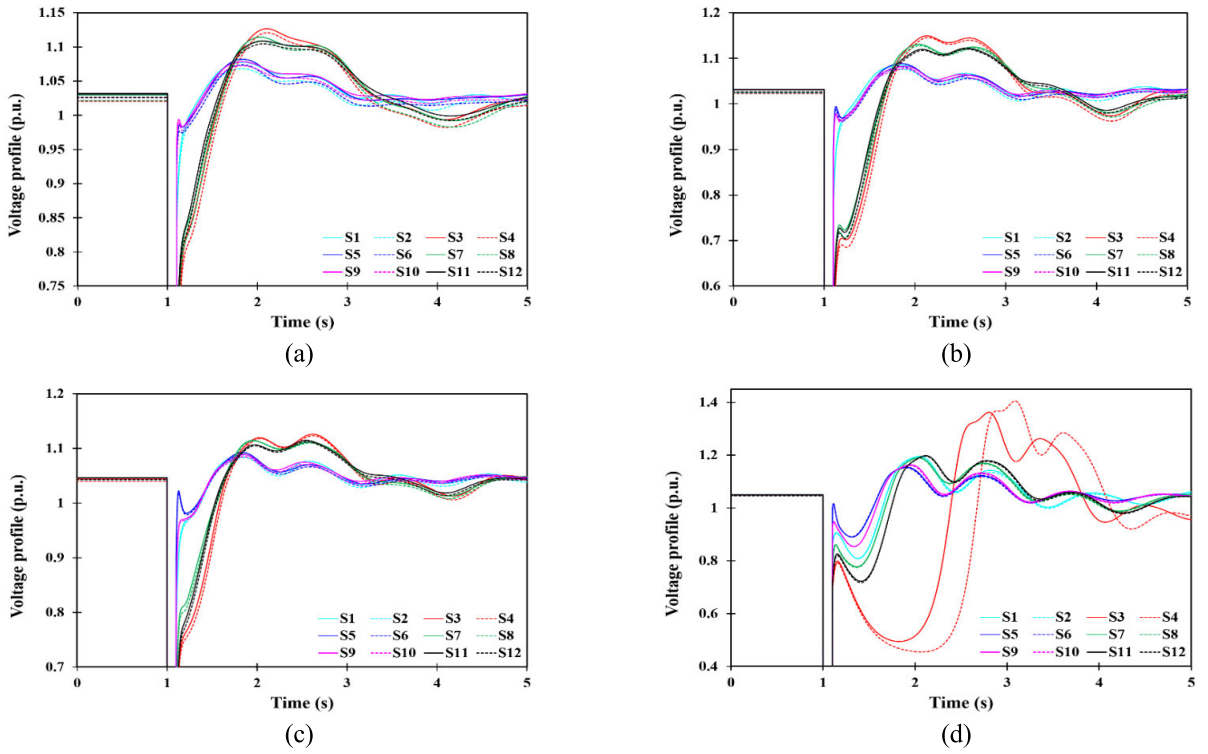

FIGURE 13. Load bus voltage profiles: (a) Bus 3, (b) Bus 16, (c) Bus 23, and (d) Bus 29.

In the base case (with static load), the buses have a wide range of VRI. Zone 1 loads have the lowest VRIs while, Zone 2 and 3 have better and similar VRIs. The dynamic loads cause the VRIs to be reduced remarkably at Bus 29 and Bus 16, respectively. However, Bus 29 and 16 represent the lowest and highest SC MVA levels, respectively. Therefore, their transient performance indicates that voltage recovery and SC MVA level are not strongly correlated. It is also observed that unlike the static load, VAr growth of dynamic load would impact bus voltage recoveries. The VRIs are improved for all buses by integrating LSPV. Compared to a static load, more enhancements in the system's transient stability are seen with dynamic loads. Moreover, Zone 1 is benefited the most after the integration of LSPV. For instance, the VRI of Bus 29 improved from 0.15 to 0.62 (400%) with 20% PV. The last simulation group involves the integration of LSPV power plants at each zonal load center through a 50 km transmission line. The LSPV has a positive influence on most loads. Nevertheless, Bus 28 and 29 VRIs are reduced slightly (about 5%) for Group C in compression to Group B. the reason for such reduction is due to the change in PV integration location.

Fig. 13 shows the voltage profile of four load buses. Bus 29, 3, and 23 represent Zone 1, 2, and 3, respectively. Bus 16 is also selected as it represents the highest short circuit level. On the other hand, Bus 29 represents the lowest short circuit level bus. These voltage profiles would explain dynamic load percentages and VAr growth influence on system transient performance. Furthermore, voltage profiles of load buses demonstrate the effect of LSPVs integration and their locations on the system post fault response.

In general, dynamic load scenarios cause a delay in voltage recovery, followed by a voltage swell for a few seconds. The load VAr growth has a slight effect on the bus post fault response, excluding Bus 29 with the LSPV, as shown in Fig. 13 (d). Generally, LSPV integration helps load buses to recover faster. Integration location plays an important role in recovery, as realized for Bus 29. The influence of PV integration (especially with dynamic load) can be seen during the first few cycles after the fault clearance, as depicted in Fig. 14. The VRT is reduced for scenarios in groups B and C with compared to Group A. The reduction in VRT means a faster voltage recovery and a lower chance of FIDVR. The improvement in system recovery emphasizes the role of PV in enhancing system short-term voltage stability. More details about the sources of sub-transient and transient VAr contributions are discussed in the next sections.

B. SUB-TRANSIENT VAr

Once a three-phase fault occurs at a load bus, the VAr sources would immediately inject a fault current to recover the voltage. The VAr injected during the fault is known as ST-VAr. The amount of the ST-VAr contribution varies among the VAr sources. It is governed by the VAr capability of the sources and the electrical distance from the fault. In the New England system, there are three VAr sources: SGs,

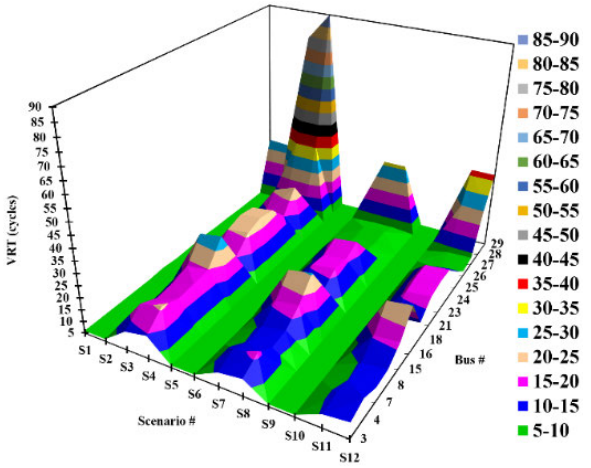

FIGURE 14. Voltage recovery time for all scenarios.

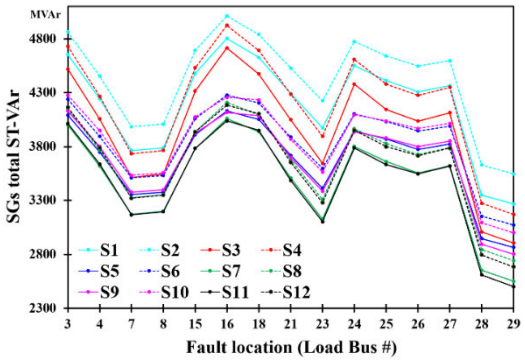

FIGURE 15. Total sub-transient VAr of SGs.

PVs (Groups B and C), and line capacitances. Fig. 15 shows the SGs total ST-VAr injected from SGs for each fault and under all the simulation scenarios. The fault location plays a major role in the ST-VAr contribution. For instance, when the fault occurs at Bus 29, SGs would inject the ST-VAr, which is 68% of SGs ST-VAr for the fault at Bus 16. This is clearly due to the influence of electrical distance from VAr sources and the load size on ST-VAr. The VAr demand growth affects the ST-VAr, in which a 4% - 9% increase occurs in ST-VAr of SGs when the load VAr is increased by 20%. The load types also influence the required amount of ST-VAr, as presented in Fig. 16.

Static and dynamic loads have different Volt–VAr behavior during the sub-transient period, as shown in Fig. 17 and 18. During the sub-transient period, the dynamic loads' VAr demand would drop significantly. This reduction would affect the ST-VAr contortions of SGs by 3% - 11% (depending on fault location). On the other hand, the total VAr consumption for static loads is reduced slightly (depending on the fault location) during the sub-transient period. Then, the VAr consumption returns to its pre-fault conditions once the fault is cleared. Conversely, with dynamic loads, an overshoot VAr consumed is observed at the beginning of the transient period (about 1 second). The contributions of SGs in Group B and C

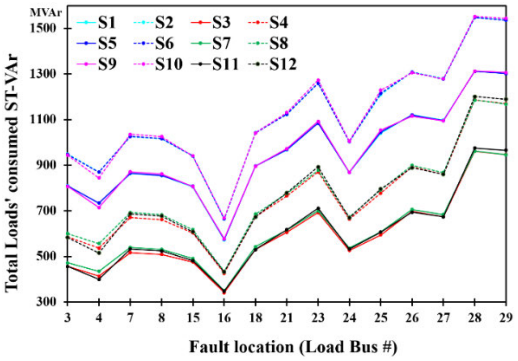

FIGURE 16. Total sub-transient VAr consumption by loads.

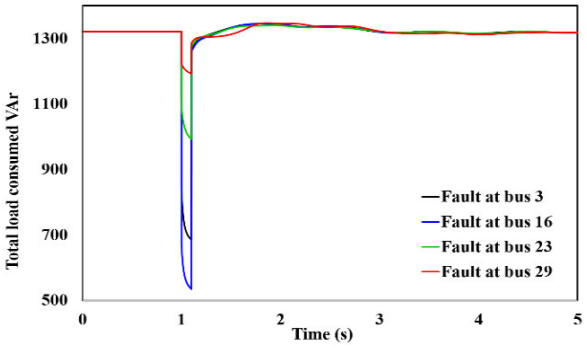

FIGURE 17. Static load VAr profiles for different fault locations.

scenarios are reduced when compared to those in Group A. This happened due to the 20% reduction of MVA ratings as the SG units are replaced by LSPVs.

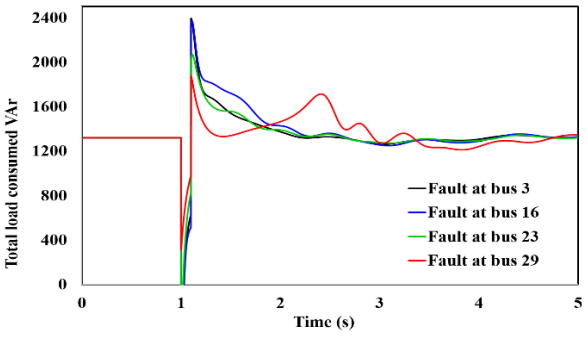

FIGURE 18. Dynamic load VAr profiles for different fault locations.

LSPV power plants have the capability to contribute to the system ST-VAr. Fig. 19 illustrates the total ST-VAr contribution from PVs for Group B and C simulation scenarios. It should be worth noting that the contribution of PVs during the sub-transient period is lower than the contribution of SGs. For instance, in scenario 4, 20% PV contributes to ST-VAr with 400 MVAr, while 80% SG contributes 4130 MVAr.

The result indicates that SGs contributed 2.6 times more than PVs. The contribution pattern of PVs in terms of fault location is similar to that of the SGs in group B scenarios.

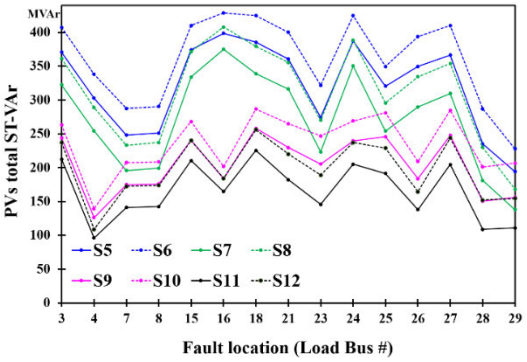

FIGURE 19. Total sub-transient VAr of PVs.

However, the last group of simulations has a different pattern of contribution. The PV integration location influences the contribution from the PV plant, as depicted in Fig. 19. The PV contributions in Group C are reduced approximately by 40% in comparison to Group B.

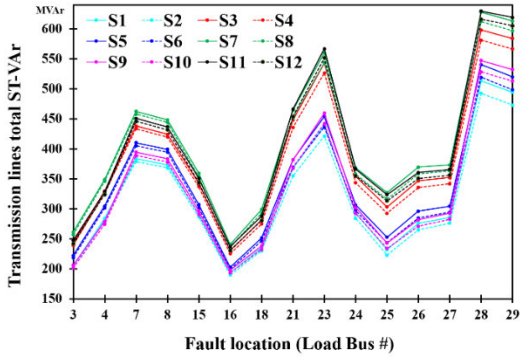

FIGURE 20. Total sub-transient VAr in line capacitances.

The third source of VAr is transmission line capacitance. Fig. 20 shows the line sub-transient contribution under the performed simulation cases. The total line ST-VAr has an opposite trend compared to ST-VAr of SGs and PVs ST-VAr. The fault location highly influenced the line VAr since this VAr is proportional to the square of the bus voltage. If a fault occurs at a strong load bus, it means the system voltage profile would be affected by that fault, and their voltages would be reduced from pre-fault values. This would result in a lower line capacitance VAr. The load VAr growth is slightly affecting the line ST-VAr. On the other hand, load types have a strong impact online performance, especially on the weakest buses. PV integration improves the line contributions. However, the integration location could slightly affect the line ST-VAr.

Table 5 summarizes the system total injected ST-VAr with the first scenario (S1) taken as a reference. For all scenarios, the 20% VAr growth results in a 4% - 7% increase in the total ST-VAr.

The dynamic load requires 2% -7% less ST-VAr when compared to the static load. PV integration at the HV side

TABLE 5. Variation in Sub-Transient VAr (total).

Fault @	Scenarios											
	S1	S2	S3	S4	S5	S6	S7	S8	S9	S10	S11	S12
Bus03	100%	104%	98%	102%	96%	100%	94%	98%	94%	98%	92%	96%
Bus04	100%	105%	97%	101%	96%	100%	93%	97%	93%	96%	90%	93%
Bus07	100%	105%	95%	100%	97%	101%	92%	97%	95%	100%	91%	95%
Bus08	100%	105%	95%	101%	97%	101%	92%	97%	95%	100%	91%	95%
Bus15	100%	104%	98%	102%	96%	100%	94%	98%	94%	97%	91%	95%
Bus16	100%	104%	99%	103%	95%	98%	94%	97%	90%	93%	89%	92%
Bus18	100%	104%	98%	102%	96%	100%	94%	98%	94%	98%	92%	95%
Bus21	100%	105%	96%	101%	96%	100%	92%	96%	92%	97%	89%	93%
Bus23	100%	105%	95%	100%	94%	99%	89%	93%	92%	96%	86%	91%
Bus24	100%	104%	98%	102%	96%	100%	93%	97%	92%	96%	90%	94%
Bus25	100%	105%	96%	101%	96%	100%	91%	96%	94%	98%	89%	93%
Bus26	100%	105%	96%	101%	96%	101%	92%	96%	93%	97%	88%	92%
Bus27	100%	105%	96%	101%	97%	101%	93%	97%	94%	99%	90%	94%
Bus28	100%	107%	93%	100%	96%	102%	90%	95%	93%	99%	87%	92%
Bus29	100%	107%	93%	99%	95%	101%	88%	93%	93%	99%	86%	92%

of SGs injects about 4% less ST-VAr when compared to the base case. However, connecting PV to the load centers through 50 km transmission lines would alter the system power flow and result in 5% -10% less ST-VAr than the base case. The ST-VAr contributes towards a better system recovery after clearing the fault. The next section highlights the system performances in the transient period that started after the fault clearance.

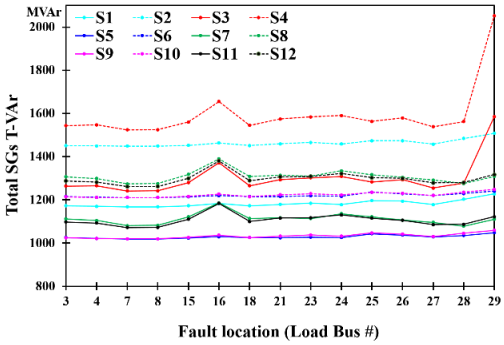

FIGURE 21. Total injected transient VAr of SGs.

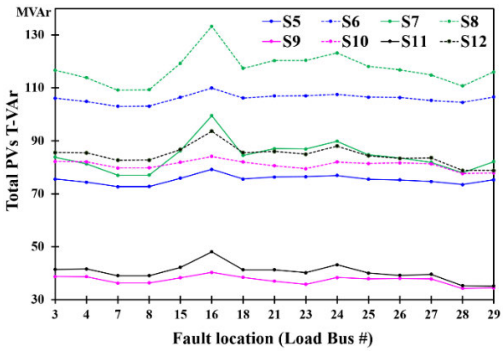

FIGURE 22. Total injected transient VAr of PVs.

C. TRANSIENT VAr

Once the disturbance is removed (after 100 ms in this examination), the system starts to recover. Faster recovery means sufficient VAr being injected to the fault. On the other hand,

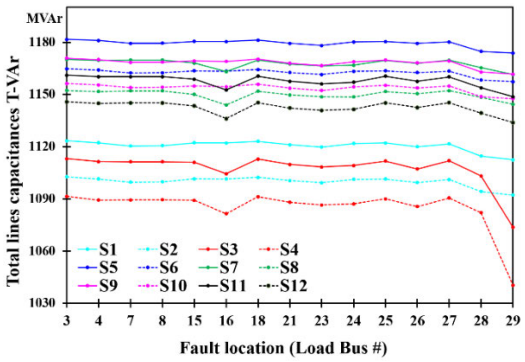

FIGURE 23. Total injected transient VAr from line capacitances.

delayed recovery is an indication of insufficient VAr on the grid. Figs. 21-23 shows the total injected VAr from SGs, PVs, and line capacitances under different operating conditions. Generally, unlike the ST-VAr, the total amounts of injected T-VAr are independent of fault locations. The total T-VAr from SGs is influenced by load VAr growth, where a 17% - 24% increase in injected VAr from SGs is observed with 20% load VAr growth. Dynamic loads affect the total T-VAr contribution of SGs by 5-36% based on the fault location. However, the LSPV integration would reduce the impact of dynamic loads to approximately 3% - 12%. The line capacitance contributes heavily towards T-VAr. More contribution (about 5%) would exist with PV integration scenarios. Conversely, with the VAr growth, the line contribution is unlike the SGs or PVs (where the T-VAr contribution would be reduced by about 2%).

Table 6 summarizes the total T-VAr variation from the base case. Unlike the total ST-VAr, the dynamic loads required more T-VAr. More VAr is required because of the overshoot in load VAr after the fault clearance, as presented in Fig. 18. The PV integration location also affects the total T-VAr, where less VAr is injected when PVs are connected to the load centers through transmission lines.

TABLE 6. Variation in transient Var (Total).

Fault @	Scenarios											
	S1	S2	S3	S4	S5	S6	S7	S8	S9	S10	S11	S12
Bus03	100%	111%	104%	115%	99%	108%	103%	112%	97%	107%	100%	110%
Bus04	100%	111%	104%	115%	99%	108%	103%	112%	97%	107%	100%	110%
Bus07	100%	111%	103%	114%	99%	108%	102%	111%	97%	107%	99%	109%
Bus08	100%	111%	103%	114%	99%	108%	102%	111%	97%	107%	99%	109%
Bus15	100%	111%	104%	115%	99%	108%	104%	113%	97%	107%	101%	110%
Bus16	100%	111%	107%	119%	99%	108%	106%	116%	97%	107%	103%	113%
Bus18	100%	111%	104%	115%	99%	108%	103%	112%	97%	107%	100%	110%
Bus21	100%	111%	104%	116%	99%	108%	103%	112%	97%	107%	101%	110%
Bus23	100%	111%	105%	116%	99%	108%	103%	112%	97%	107%	100%	110%
Bus24	100%	111%	105%	116%	99%	108%	104%	113%	97%	107%	101%	111%
Bus25	100%	111%	103%	114%	99%	108%	102%	112%	97%	107%	100%	109%
Bus26	100%	111%	104%	115%	99%	108%	102%	111%	97%	107%	99%	109%
Bus27	100%	111%	103%	114%	99%	108%	102%	111%	97%	107%	99%	109%
Bus28	100%	111%	103%	114%	99%	108%	100%	109%	97%	106%	98%	108%
Bus29	100%	111%	114%	132%	98%	107%	101%	110%	96%	106%	99%	108%

D. PERFORMANCE SUMMARY

The system sub-transient and transient performance is critical for system stability. The contribution of VAr sources is essential. However, they have different participation in E-VAr. Table 7 shows the average contribution of each VAr source out of the total injected VAr in the sub-transient and transient time frames. SGs are the primary source of ST-VAr. However, fault location influence could limit the contribution of SGs. In such a case, line capacitance share increased to 12% and 15%, respectively. The PV power plants represent 20% of system MVA. However, they inject 5% - 7% of the system's total ST-VAr due to their limited fault current contribution.

After the fault is cleared, the share of VAr resources in total T-VAr is significantly changed. The contribution is less sensitive to the fault location. The SGs inject more than half of T-VAr. Line capacitances are the second source and contribute to T-VAr. The PVs have a low share of T-VAr. However, this is not representing PV maximum VAr capability rather than the influence of voltage control set-point.

TABLE 7. VAr sources participation factor in the total ST-VAr and T-VAr.

Faulted Bus#	Sub-transient VAr			Transient VAr		
	SGs	PVs	lines	SGs	PVs	lines
Bus03	91%	6%	5%	50%	3%	47%
Bus04	90%	5%	7%	50%	3%	47%
Bus07	86%	5%	10%	50%	3%	48%
Bus08	86%	5%	10%	50%	3%	48%
Bus15	89%	7%	7%	51%	3%	47%
Bus16	91%	6%	4%	51%	3%	46%
Bus18	90%	7%	6%	50%	3%	47%
Bus21	86%	7%	9%	51%	3%	47%
Bus23	84%	6%	12%	51%	3%	47%
Bus24	88%	7%	7%	51%	3%	47%
Bus25	90%	6%	6%	51%	3%	47%
Bus26	89%	6%	7%	51%	3%	47%
Bus27	88%	7%	7%	50%	3%	47%
Bus28	81%	5%	15%	51%	3%	47%
Bus29	81%	5%	15%	52%	3%	46%

VI. CONCLUSION

In this paper, each VAr source contribution towards the system effective VAr (E-VAr) has comprehensively been assessed. These analyses considered the system responses during the steady-state, sub-transient, and transient time frame to determine the E-VAr under different operating conditions. The VAr sources considered in this research are synchronous generators (SGs) with the detailed model, PV inverters with fixed d and q current limit, and transmission lines with nominal Pi (Π) model. The influence of fault locations, load types, load VAr growth, PV integration locations, and penetration levels on the E-VAr has been explored. A framework for assessing the contribution in the E-VAr is presented and assessed in this paper using a multi-area test power system.

From the results, it is observed that all the VAr sources have contributed towards different amounts of E-VAr. However, SGs are the main source of reactive power during and after the disturbance. Moreover, the fault location has a major

impact on the E-VAr contribution of SGs that would result in different voltage recovery for each load bus. The load bus short circuit MVA level is highly correlated with SGs ST-VAr. On the other hand, bus VRIs are more correlated to the T-VAr of SGs. The load types would also affect the sub-transient and transient performance, while the VAr demand growth may have less impact on post-fault performances of most buses in the system. The investigation also highlights the role of transmission line capacitance on system post-fault performance. Transmission line capacitances contribute heavily to the T-VAr. The line contribution is sensitive to the fault locations as the line VAr is proportional to the square of line voltage. Additionally, the PV integration locations would affect transmission line net VAr. Therefore, affects the system's post-fault performance. An optimal integration location of IBRs would help the transmission system operators to host more renewable energy without compromising system stability.

ACKNOWLEDGMENT

S. Alzahrani would like to thank Al Baha University, Saudi Arabia, for sponsoring his postgraduate study at The University of Queensland, Brisbane, QLD, Australia.

REFERENCES

[1] R. Shah, N. Mithulananthan, R. C. Bansal, and V. K. Ramachandaramurthy, "A review of key power system stability challenges for large-scale PV integration," *Renew. Sustain. Energy Rev.*, vol. 41, pp. 1423–1436, Jan. 2015.

[2] L. Meegahapola and T. Littler, "Characterisation of large disturbance rotor angle and voltage stability in interconnected power networks with distributed wind generation," *IET Renew. Power Gener.*, vol. 9, no. 3, pp. 272–283, Apr. 2015.

[3] H. Gu, R. Yan, and T. Saha, "Review of system strength and inertia requirements for the national electricity market of Australia," *CSEE J. Power Energy Syst.*, vol. 5, no. 3, pp. 295–305, Sep. 2019.

[4] G. Lammert, D. Premm, and L. D. P. Ospina, "Control of photovoltaic systems for enhanced short-term voltage stability and recovery," *IEEE Trans. Energy Convers.*, vol. 34, no. 1, pp. 243–254, Mar. 2019.

[5] B. Y. Qi, K. N. Hasan, and J. V. Milanovic, "Identification of critical parameters affecting voltage and angular stability considering load-renewable generation correlations," *IEEE Trans. Power Syst.*, vol. 34, no. 4, pp. 2859–2869, Jul. 2019.

[6] J. F. Zhang, C. Y. Chung, C. T. Tse, and K. W. Wang, "Voltage stability analysis considering the uncertainties of dynamic load parameters," *IET Gener., Transmiss. Distrib.*, vol. 3, no. 10, pp. 941–948, Oct. 2009.

[7] Y. H. Choi, S. Seo, S. Kang, and B. Lee, "Justification of effective reactive power reserves with respect to a particular bus using linear sensitivity," *IEEE Trans. Power Syst.*, vol. 26, no. 4, pp. 2118–2124, Nov. 2011.

[8] M. Paramasivam, A. Salloum, and V. Ajjarapu, "Dynamic optimization based reactive power planning to mitigate slow voltage recovery and short term voltage instability," *IEEE Trans. Power Syst.*, vol. 28, no. 4, pp. 3865–3873, Nov. 2013.

[9] G. Lammert, Modelling, Control and Stability Analysis of Photovoltaic Systems in Power System Dynamic Studies. Kassel: Kassel University Press GmbH, 2019, p. 202.

[10] R. K. Varma and S. Mohan, "Mitigation of fault induced delayed voltage recovery (FIDVR) by PV-STATCOM," *IEEE Trans. Power Syst.*, vol. 35, no. 6, pp. 4251–4262, Nov. 2020.

[11] K. Kawabe, Y. Ota, A. Yokoyama, and K. Tanaka, "Novel dynamic voltage support capability of photovoltaic systems for improvement of short-term voltage stability in power systems," *IEEE Trans. Power Syst.*, vol. 32, no. 3, pp. 1796–1804, May 2017.

[12] B. Park, S. Im, D. Kim, and B. Lee, "Clustered effective reactive reserve to secure dynamic voltage stability in power system operation," *IEEE Trans. Power Syst.*, vol. 36, no. 2, pp. 1183–1192, Mar. 2021.

[13] T. Niu, Q. Guo, H. Sun, H. Liu, B. Zhang, and Y. Du, "Dynamic reactive power reserve optimisation in wind power integration areas," *IET Gener., Transmiss. Distrib.*, vol. 12, no. 2, pp. 507–517, Jan. 2018.

[14] E. E. El-Araby and N. Yorino, "Reactive power reserve management tool for voltage stability enhancement," *IET Gener., Transmiss. Distrib.*, vol. 12, no. 8, pp. 1879–1888, Apr. 2018.

[15] D. Yang, H. Cheng, Z. Ma, L. Yao, and Z. Zhu, "Dynamic VAR planning methodology to enhance transient voltage stability for failure recovery," *J. Mod. Power Syst. Clean Energy*, vol. 6, no. 4, pp. 712–721, Jul. 2018.

[16] R. Shah and N. Mithulananthan, "Test systems for dynamic stability studies in electric power system," in *Proc. Australas. Universities Power Eng. Conf. (AUPEC)*, Sep. 2013, pp. 1–6.

[17] R. Liu, J. Yao, X. Wang, P. Sun, and J. Pei, "Dynamic stability analysis and improved LVRT schemes of DFIG-based wind turbines during a symmetrical fault in a weak grid," *IEEE Trans. Power Electron.*, vol. 35, no. 1, pp. 303–318, Jan. 2020.

[18] *WECC Solar Plant Dynamic Modeling Guidelines*, WECC Renewable Energy Modeling Task Force, Salt Lake City, UT, USA, 2014.

[19] K. W. Jones, "Impact of inverter based generation on bulk power system dynamics and short-circuit performance," Inst. Elect. Electron. Eng., New York, NY, USA, Tech. Rep. PESTR68, Jul. 2018.

[20] *National Electricity Rules_Version 126*, AEMC, Sydney, NSW, Australia, Nov. 2019.

[21] A. Q. Al-Shetwi, M. A. Hannan, K. P. Jern, M. Mansur, and T. M. I. Mahlia, "Grid-connected renewable energy sources: Review of the recent integration requirements and control methods," *J. Cleaner Prod.*, vol. 253, Apr. 2020, Art. no. 119831.

[22] L. G. Kong, G. W. Cai, S. Xue, and S. H. Li, "Modeling and coordinated control strategy of large scale grid-connected wind/photovoltaic/energy storage hybrid energy conversion system," *Math. Problems Eng.*, vol. 2015, Jan. 2015, Art. no. 682321.

[23] S. Alzahrani, R. Shah, N. Mithulananthan, and A. Sode-Yome, "Large-scale PV voltage regulation: Survey of recent practice," in *Proc. IEEE PES GTD Grand Int. Conf. Expo. Asia (GTD Asia)*, Mar. 2019, pp. 661–666.

[24] J. Milanovic, S. Djokic, and J. Matevosyan, "Modelling and aggregation of loads in flexible power networks," CIGRE, Paris, France, Tech. Rep. WG C4.605, Feb. 2014.

[25] J. V. Milanovic, K. Yamashita, S. Martinez Villanueva, S. Z. Djokic, and L. M. Korunovic, "International industry practice on power system load modeling," *IEEE Trans. Power Syst.*, vol. 28, no. 3, pp. 3038–3046, Aug. 2013.

[26] *A Technical Reference Paper Fault-Induced Delaed Voltage Recovery*, Transmiss. Issues Subcommittee Syst. Protection Control Subcommittee, NERC, Princeton, NJ, USA,Jun. 2009.

[27] Y. Zhu, J. V. Milanović, and K. N. Hasan, "Ranking and quantifying the effects of load model parameters on power system stability," *IET Gener., Transmiss. Distrib.*, vol. 13, no. 20, pp. 4650–4658, Oct. 2019.

[28] Y. Zhu, "Ranking of power system loads based on their influence on power system stability," Ph.D. Dissertation, School Elect. Electron. Eng., Univ. Manchester, Manchester, U.K., 2019.

[29] K. Kawabe and K. Tanaka, "Analytical method for short-term voltage stability using the stability boundary in the P-V plane," *IEEE Trans. Power Syst.*, vol. 29, no. 6, pp. 3041–3047, Nov. 2014.

[30] A. Alshareef, R. Shah, N. Mithulananthan, and S. Alzahrani, "A new global index for short term voltage stability assessment," *IEEE Access*, vol. 9, pp. 36114–36124, 2021.

[31] D. J. Shoup, J. J. Paserba, and C. W. Taylor, "A survey of current practices for transient voltage dip/sag criteria related to power system stability," in *Proc. IEEE PES Power Syst. Conf. Expo.*, vol. 2, Oct. 2004, pp. 1140–1147.

[32] H. Saadat, *Power System Analysis*. New York, NY, USA: McGraw-Hill, 1999.

S. ALZAHRANI (Member, IEEE) received the B.Sc. degree in engineering from the King Fahd University of Petroleum & Minerals (KFUPM), Saudi Arabia, in 2009, and the M.Eng. degree from The University of Queensland, Brisbane, QLD, Australia, in 2015, where he is currently pursuing the Ph.D. degree with the Power, Energy and Control Engineering Research Group, School of Information Technology and Electrical Engineering. His research interests include large-scale renewable energy integration, and power system stability studies.

RAKIBUZZAMAN SHAH (Member, IEEE) received the M.Eng. degree from the Asian Institute of Technology, Bangkok, Thailand, and the Ph.D. degree from the University of Queensland, Australia. Before joining FedUni Australia, he had worked with The University of Manchester, The University of Queensland, and Central Queensland University. He is currently a Senior Lecturer in smart power systems engineering with the School of Engineering Information Technology and Physical Sciences, Federation University Australia (FedUni Australia). He has experience working at, and consulting with, DNOs and TSOs on individual projects and collaborative work on a large number of projects, primarily on the dynamic impact of integrating new technologies and power electronics into large systems. He has more than 80 international publications (journals and conferences) and has spoken at the leading power system conferences around the world. His research interests include future power grids, such as renewable energy integration and wide-area control, asynchronous grid connection through VSC-HVDC, power system stability and dynamics, application of data mining in power systems, application of control theory in power systems, distribution system energy management, and low carbon energy systems.

N. MITHULANANTHAN (Senior Member, IEEE) received the B.Sc. (Eng.) degree from the University of Peradeniya, Sri Lanka, the M.Eng. degree from the Asian Institute of Technology (AIT), Bangkok, and the Ph.D. degree from the University of Waterloo, Waterloo, ON, Canada. He has been the Director of the Higher Degree Research Training and a Post Graduate Coordinator with the School of Information Technology and Electrical Engineering, The University of Queensland, since July 2019. Prior to joining The University of Queensland, he was attached to Energy Field of Study at AIT. His previous professional positions include a Planning Engineer at the Generation Planning Division for two years at Ceylon Electricity Board, Sri Lanka, and a Project Leader at the Centre of Excellence in Electric Power Technology for one year at Chulalongkorn University, Thailand. His research interests include analytical studies on electric power grids, power system stability and dynamics, grid integration of renewable energy, battery energy storage, and electric vehicle charging stations.